



# Thermal degradation kinetics of ionic liquid [BMIM]BF<sub>4</sub>/TEA/PFSA composite membranes for fuel cell

Yi-heng Lu<sup>1</sup> · Kang Li<sup>1</sup> · Yu-wei Lu<sup>2</sup> · Wen-quan Feng<sup>1</sup>

Received: 29 July 2017 / Accepted: 4 October 2018 / Published online: 19 October 2018  
© Akadémiai Kiadó, Budapest, Hungary 2018

## Abstract

20% ILs-TEA-PFSA composite membranes were prepared using the ionic liquid 1-butyl-3-methylimidazolium tetrafluoroborate [BMIM]BF<sub>4</sub> (ILs) and were doped with triethylamine (TEA) to modify the perfluorosulfonic acid (PFSA). The thermal decomposition kinetics of the composite membrane was investigated using nonisothermal thermogravimetry in order to study the high-temperature durability of the ionic-liquid-doped industrial-grade perfluorosulfonic acid ion membrane for fuel cells. The results showed that the thermal degradation of the composite membranes occurs over three stages, for which the conversion rates are in the ranges of 0.01–0.1, 0.15–0.4 and 0.45–0.7. The average apparent activation energies of membrane degradation in the first, second and third stages are 151.3, 166.5 and 170.1 kJ mol<sup>-1</sup>, respectively. At a heating rate ( $\beta$ ) of 20 °C min<sup>-1</sup>, the thermal degradation process of the composite mechanism follows an  $n=4$  reaction order mechanism, and the mechanism function  $f(\alpha)$  is  $1-(1-\alpha)^4$  and  $g(\alpha)$  is  $1/4(1-\alpha)^{-3}$ . The heat resistance showed that if  $\beta$  is equal to 15 °C min<sup>-1</sup>, the lowest temperature at which the composite membrane decomposes by 1% is 363.5 °C. Similarly, when  $\alpha$  is 0.32%, the thermal decomposition of the composite membrane occurs above 350 °C. Isothermal thermogravimetric analysis showed that the thermal lifetimes ( $t_{5\%}$  and  $t_{10\%}$ ) of the composite membrane were  $4.83 \times 10^5$  and  $9.80 \times 10^5$  h, respectively. If  $\alpha$  reached 5 and 10% under a nitrogen atmosphere at 180 °C, the isothermal decomposition process underwent a first-order reaction mechanism. The apparent activation energy ( $E_a$ ) of the thermal degradation of the composite membrane was 166.8 kJ mol<sup>-1</sup>. In addition, using isothermal data from a 20% [BMIM] BF<sub>4</sub>/TEA/PFSA composite membrane at 688 K, based on a first-order reaction, the respective theoretical master curves were compared with the experimental master plots of  $da/d\theta/(da/d\theta)_{\alpha=0.5}$ ,  $\theta/\theta_{0.5}$  and  $(da/d\theta)_0$  versus  $\alpha$ .

**Keywords** 1-Butyl-3-methylimidazolium tetrafluoroborate · Perfluorinated sulfonic acid · Composite membrane · Thermal degradation kinetics · Thermal life

## Introduction

In recent years, the introduction of ionic liquids into polymer electrolyte membranes has been a very active research topic [1–3]. Ionic liquids are molten salts composed of organic cations and inorganic anions and have excellent proton conductivity, heat resistance and chemical stability. In addition, they are nonvolatile and

environmentally friendly and are suitable for proton exchange membrane fillers under dry conditions at high temperature. The research is as follows.

Hybrid membranes are prepared by combining substrates such as SPI, polyimide, PEEK, PVDF, PBI, and ABPBI with ionic liquids such as [Dema]TfO, [C4im], [C4im][BEHP], HMI-Tf, etc., in order to improve the conductivity of the composite membranes. A modified sulfonated polyimide (SPI) composite membrane was prepared using a proton ionic liquid, which greatly improved the conductivity of the proton exchange membrane. In the SPI/IL composite membrane, when the ionic liquid mass ratio was 50 mass%, the proton conductivity could reach 3–6 mS cm<sup>-1</sup> [4] under dry conditions at 120 °C. The proton-type ionic liquid [Dema]TfO can be

✉ Yi-heng Lu  
yhlu@aust.edu.cn

<sup>1</sup> College of Chemical Engineering, Anhui University of Science and Technology, Huainan 232001, China

<sup>2</sup> Laboratoire de Chimie Physique, Université de Paris Sud, 91405 Orsay Cedex, France

used as a proton conductor for  $H_2/O_2$  fuel cells, which can operate at temperatures above 100 °C without humidification [5]. A functionalized graphene [FGO]/sulfonated polyimide (SPI) composite proton exchange membrane was synthesized with a phosphoric acid-doped ionic liquid and had a proton conductivity at 120 °C and 80% relative humidity of  $0.1243 \text{ S cm}^{-1}$  [6]. 1-*n*-butyl imidazolyl dibutyl phosphate (DBI) [C<sub>4</sub>im], [DBP] and 1-*n*-butyl imidazole bis-2-methyl-ethylhexyl phosphate ([C<sub>4</sub>im] [BEHP]) were combined with a polyimide composite membrane for high-temperature fuel cell testing [7].

A proton-inert ionic liquid and sulfonated polyether ether ketone were cross-linked into a complex anhydrous proton-conducting membrane for fuel cells at a temperature of 30–140 °C in anhydrous conditions, and the proton conductivity of the material reached  $10^{-3} \text{ S cm}^{-1}$  [8].

An imidazole ionic liquid and sulfonated polyether ether ketone were prepared and the thermal stability of the composite membrane reached 340 °C. At an increased temperature, the ionic conductivity reached  $8.3 \times 10^{-3} \text{ S cm}^{-1}$  [9]. Other ionic liquids can also enhance the anhydrous proton conductivity of polymer electrolyte membranes [10].

In the phosphoric acid-doped imidazole ionic liquid polymer composite membrane, the phosphoric acid composition plays a major role in the proton conduction of the composite membrane, and an SPEEK/50% BMIMPF<sub>6</sub>/4.6PA membrane used at 160 °C in anhydrous conditions had a maximum proton conductivity of  $3.0 \times 10^{-2} \text{ S cm}^{-1}$  [11].

A novel composite membrane was prepared by embedding methacrylic acid polyelectrolyte microcapsules (PMCs) into sulfonated polyetheretherketone (SPEEK) and then immersing the imbedded polymer into imidazole ionic liquids [12]. A new type of anhydrous proton membrane was prepared using ionic liquid trifluoroacetate (TFAPA) and sulfonated polyetheretherketone (SPEEK) or polyvinylidene fluoride (PVDF) [13]. In addition, ionic liquid oxide graphite/polybenzimidazole composite membrane (ILGO/PBI) have been reported [14]; PBI/IL composite membranes were synthesized using polybenzimidazole (PBI) and 1-hexyl-3-methylimidazole trifluoromethanesulfonic acid (HMI-Tf) ionic liquids [15]. By adding benzimidazolyl ionic liquid 1-butyl-3-ethylbenzimidazole dihydrogen phosphate (BEBzIm- $H_2PO_4$ ) into the ABPBI- $H_3PO_4$  proton exchange membrane, the membrane could be used for a fuel cell at a temperature of above 100 °C [16]. The modified polybenzimidazole membrane was prepared using 1-H-3-methylimidazole bis-trifluoro-methanesulfonyl imide salt ion liquid for high-temperature fuel cell testing. The conductivity of PBI/IL membrane reached  $1.86 \text{ mS cm}^{-1}$  at 190 °C, and its

performance in the fuel cell was better than that of Nafion117 [17].

The thermal and thermo-oxidative degradation of poly(2,6-dimethyl-1,4-phenylene oxide) (PPO)/copoly(aryl ether sulfone) P(ESES-co-EES) block copolymers were investigated using a kinetic study [18]. The chemical stability of BaCeO<sub>3-δ</sub>-based protonic conductors was measured using a DTA-TG-MS technique [19]. The thermal energy storage and retrieval properties of form-stable phase-changing nanofibrous mats based on ternary fatty acid eutectics/polyacrylonitrile composites were studied by magnetron sputtering of silver [20]. The physical and chemical nature of the low- to high-proton-conducting transformation of a CsHSO<sub>4</sub>-CsH<sub>2</sub>PO<sub>4</sub> solid solution and its parents were studied [21]. DSC studies on a sulfonated tetrafluoroethylene-based fluoropolymer copolymer (Nafion) and cellulose biopolymer materials were reviewed [22]. Ceramic tape including Ca<sub>0.05</sub>Ba<sub>0.95</sub>Ce<sub>0.9</sub>Y<sub>0.1</sub>O<sub>3</sub> as an electrolyte for electrolyte-supported solid oxide fuel cells (IT-SOFCs) have been designed, and their physicochemical properties were discussed [23]. Ternary nanotubes of MnO<sub>2</sub>/GO/AC were synthesized as an excellent alternative composite modifier for the cathode electrode of microbial fuel cells [24]. Three-dimensional computational fluid dynamic modeling was constructed for a proton exchange membrane electrolyzer with new flow field patterns [25]. Polymer electrolytes containing solvate ionic liquids, a new approach to achieve high ionic conductivities, thermal stabilities, and wide potential windows, were reported [26]. Ionic-liquid-modified poly(vinyl alcohol) was constructed with improved thermal processability and electrical conductivity of  $2.82 \times 10^{-3} \text{ S cm}^{-1}$  [27]. Polymer inclusion membranes (PIMs) containing phosphonium ionic liquids as Zn(II) carriers were characterized [28]. An organic-inorganic composite membrane based on sulfonated poly(arylene ether ketone sulfone) was prepared for proton exchange membrane fuel cells with excellent long-term stability [29]. Polybenzimidazole/ionic-liquid-functional silica composite membranes were prepared with improved proton conductivity for high-temperature proton exchange membrane fuel cells [30].

Although there have been numerous reports on the preparation and stability of ionic liquids and polymer electrolyte composite membranes in the past few decades, the improved heat resistance for hybrid membranes is far from being solved. Currently, the composite membrane is still the core component in fuel cells. Therefore, we used the common ionic liquid 1-butyl-3-methylimidazolium tetrafluoroborate ([BMIM]BF<sub>4</sub>), triethylamine (TEA) and industrial-grade membrane perfluorosulfonic acid (PFSA) for hybridization and modification in order to study the thermal stability and thermal degradation kinetics of the membranes. The synthesized composite membrane showed

excellent heat resistance, and the strength of the intermolecular forces was closely related to the difficulty of the thermal decomposition. The thermal stability and thermal degradation kinetics provide important basic information about the composite membranes and are very important for the application of the membranes to fuel cells but have never been reported in the literature.

Based on our previous work [31, 32], the nonmodel thermal degradation kinetics of the composite membrane was analyzed using nonisothermal thermogravimetry and the Kissinger method, Flynn–Wall–Ozawa method, Starink method and Friedman method. The kinetic parameters and mechanism of the membrane thermal degradation processes were obtained. In addition, using isothermal thermogravimetric data, the thermal lifetime to reach a thermal degradation of 20% for [BMIM]BF<sub>4</sub>/TEA/PFSA composite membranes was solved. When stored at 180 °C, the mass loss reached 10%, and the corresponding thermal life of the composite membrane at  $t_{10\%}$  was  $9.80 \times 10^5$  h. With a heating rate  $\beta$  of 15 °C min<sup>-1</sup>, the temperature at which the composite membrane decomposed by 1% was 363.5 °C. When heated to 350 °C, the conversion rate of the composite membrane was 0.32%. This indicates that the composite membrane has good heat resistance at high temperatures. If the decomposition process follows an isothermal first-order reaction and the conversion rate  $\alpha$  is 10%, the activation energy ( $E_a$ ) of the composite membrane is 166.8 kJ mol<sup>-1</sup>. Using the isothermal data from a 20%[BMIM]BF<sub>4</sub>/TEA/PFSA composite membrane at 688 K undergoing a first-order reaction, the theoretical master curves were compared to the experimental master plots of  $d\alpha/d\theta/(d\alpha/d\theta)_{\alpha=0.5}$ ,  $\theta/\theta_{0.5}$  and  $(d\alpha/d\theta)_0$  versus  $\alpha$  and the curves overlap well.

## Experimental

### Materials

The proton exchange membrane (perfluorosulfonic acid ion exchange membrane, referred to as PFSA), appears colorless and translucent (grade, Nepem-112; thickness, 50  $\mu$ m; tensile modulus, 630 MPa) and was purchased from the Jiangsu Huai'an Ke Run Membrane Materials Co, China. Nitric acid, ethanol and triethylamine are all of analytical grade and were used without purification. 1-Butyl-3-methylimidazolium tetrafluoroborate ionic liquid (reagent grade, referred to as ILs) was purchased from the Shanghai Chengjie Chemical Co, China.

### Thermogravimetric analysis

Thermal degradation analysis was carried out using a Shimadzu thermal analyzer, model DTG-60H, with heating rates of 15, 20 and 40 °C min<sup>-1</sup>, respectively. A platinum crucible was used under a nitrogen gas atmosphere with a flow rate of 100 mL min<sup>-1</sup> in a temperature range of 25–700 °C. Conditions for differential scanning calorimetry (DSC) were the same as above.

### Isothermal thermogravimetric analysis

For isothermal thermogravimetric analysis, the material was rapidly heated to 400 °C under a N<sub>2</sub> atmosphere and was heated isothermally at three temperatures of 410, 415 and 420 °C for 60 min. A Shimadzu thermal analyzer, model DTG-60H, was used to record the thermogravimetric results.

### TG–IR–MS analysis

Online mode TG–IR–MS analysis was performed on a TGA8000-FRONTIER-SQ8 instrument manufactured by PerkinElmer (PE), USA. The sample mass was approximately 17 mg, the carrier gas was high-purity N<sub>2</sub>, the carrier gas flow rate was 20 mL min<sup>-1</sup>, the heating rate was 20 °C min<sup>-1</sup>, the initial temperature was 35 °C, and the final heating temperature was 700 °C. High-purity helium (99.9999%) was used as the carrier gas, the transmission line temperature was 280 °C, and the inlet temperature was 280 °C. The ion source is an EI source (70 eV) and the ion source temperature is 280 °C. The  $m/z$  mass scan range is 30–200.

### Preparation of composite membranes

#### Membrane pretreatment

A PFSA membrane with a size of 1.0  $\times$  2.0 cm was surface-washed with deionized water, refluxed with 2 M nitric acid for 1 h and washed with deionized water to give PFSA H<sup>+</sup> membrane. The resulting proton membrane was placed in a (1 mol) triethylamine (TEA) ethanol solution (50/50/v/v) at room temperature for 24 h, washed with deionized water until the pH was neutral, and dried at 80 °C for 48 h to give TEA/PFSA membrane.

#### Preparation of composite membranes

Using a configuration of 20 mass% ILs ionic liquid–aqueous solution, the PFSA-TEA membrane was immersed in the above solution, sealed at 80 °C, and underwent a

constant temperature reaction for 48 h. After removal, the material was vacuum dried at 80 °C for 8 h, and the mass of the membrane was taken before and after. A 20% ILs/TEA/PFSA composite membrane was obtained. Using ILs to create triethylamine-doped perfluorosulfonic acid ion exchange membranes, a composite membrane was synthesized as shown in Scheme 1.

## Kinetic analysis

At certain temperatures, the rate of the thermal decomposition of the ionic-liquid-doped perfluorosulfonic acid composite film can be expressed by Eq. (1):

$$\frac{d\alpha}{dT} = \frac{1}{\beta} k(T) f(\alpha) \quad (1)$$

$d\alpha/dT$  is the reaction rate ( $\%K^{-1}$ ),  $k(T)$  is the temperature constant of the rate constant,  $\beta$  is the  $dT/dt$  heating rate ( $K \text{ min}^{-1}$ ), and  $f(\alpha)$  is a differential equation describing the reaction. The relationship between the rate constant  $k$  and the temperature is in accordance with the Arrhenius equation shown in Eq. (2):

$$k = A \exp\left(-\frac{E}{RT}\right) \quad (2)$$

The general equation for the thermal decomposition kinetics of the composite membrane, Eq. (3), is obtained by introducing  $\beta$  and Eq. (2) into Eq. (1):

$$\frac{d\alpha}{dt} = A \exp\left(-\frac{E}{RT}\right) f(\alpha) \quad (3)$$

where  $A$  is the pre-exponential factor ( $\text{min}^{-1}$ ),  $\alpha$  is the conversion rate (%),  $E$  is the apparent activation energy ( $\text{kJ mol}^{-1}$ ) of the reaction,  $R$  is a gas constant of  $8.314 \text{ J mol}^{-1} \text{ K}^{-1}$ , and  $T$  is the thermodynamic temperature (K). Since the ionic-liquid-doped perfluorosulfonic acid composite membrane is part of the thermal degradation of the polymer electrolyte material, it is consistent with, the Kissinger model [Eq. (5)] [33], Flynn–Wall–Ozawa model [Eq. (6)] [34], Friedman model [Eq. (7)] [35] and Starink model [Eq. (8)] [36]. Therefore, the kinetic parameters of the membrane pyrolysis can be obtained, including the apparent activation energy ( $E$ ), pre-exponential factor ( $A$ ) and linear coefficient ( $r$ ). The rate of pyrolysis of the membrane is obtained according to Eq. (4):

$$\frac{d\alpha}{dT} = \left(\frac{k}{\beta}\right) f(\alpha) \quad (4)$$

where  $k$  is the Arrhenius velocity constant/ $\text{min}^{-1}$ , according to Eq. (5), the conversion rate  $\alpha$  is:

$$\alpha = \frac{(W_i - W_t)}{W_i} \quad (5)$$

where  $W_t$  is the mass of the sample at time  $t$ , and  $W_i$  is the initial mass of the sample, Eq. (6) was obtained using the Kissinger equation:

$$\ln\left(\frac{\beta}{T_p^2}\right) = \ln\left(\frac{AR}{E}\right) - \frac{E}{RT_p} \quad (6)$$

where  $T_p$  is the peak temperature (K), and when  $\ln(\beta/T_p^2)$  is linearly related to  $1/T_p$ ,  $E$  can be obtained by the slope  $-E/R$ ; Eq. (7) was obtained using the Flynn–Wall–Ozawa method.

$$\lg \beta = \lg \left[ \frac{AE}{RG(\alpha)} \right] - 2.315 - 0.4567 \frac{E}{RT} \quad (7)$$

$G(\alpha)$  is the integral function, when  $\alpha$  is constant,  $G(\alpha)$  is constant,  $A$ ,  $E$  is fixed; If  $\lg \beta$  and  $1/T$  form linear relationship, the value of  $E$  can be obtained through the slope  $-E/R$ . For the Starink method, Eq. (8) is used:

$$\ln\left(\frac{\beta}{T^{1.8}}\right) = C_s - \frac{E}{RT} \quad (8)$$

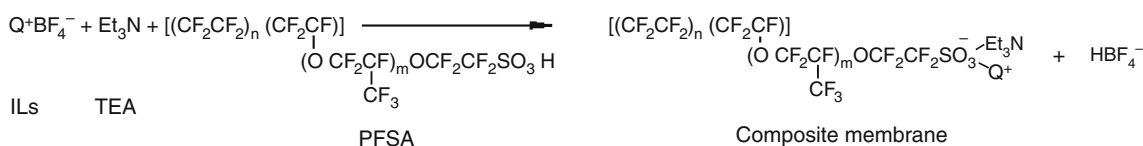
where  $C_s$  is a constant,  $\ln(\beta/T^{1.8})$  and  $1/T$  form a linear relationship, and from the slope of  $-E/R$ ,  $E$  can be obtained. Using the Friedman method, Eq. (9) is also available:

$$\ln\left(\frac{d\alpha}{dt}\right) = \ln[Af(\alpha)] - \frac{E}{RT} \quad (9)$$

When  $\alpha$  is constant,  $f(\alpha)$  is constant, and  $\ln(d\alpha/dt)$  and  $1/T$  form a linear relationship.  $E$  can be obtained from the slope of  $-E/R$ .

Since Eqs. (6), (7), (8) and (9) are model-less kinetic equations, they can be calculated without considering the calculated error of the differential and integral mechanism functions  $f(\alpha)$  and  $G(\alpha)$ , and the apparent activation energy of thermal degradation can be obtained.

Using the Achar–Brindley–Sharp differential equation (A-B-S), Eq. (10) can be obtained.



**Scheme 1** Synthesis of composite membranes using ionic-liquid-doped PFSA. Note:  $\text{Q}^+$  = 1-butyl-3-methylimidazolium cation

$$\ln\left(\frac{d\alpha}{f(\alpha)dT}\right) = \ln\left(\frac{A}{\beta}\right) - \frac{E}{RT} \quad (10)$$

where  $f(\alpha)$  is a differential function, and when  $\ln [d\alpha/f(\alpha) dT]$  is linearly related to  $1/T$ ,  $E$  can be obtained from the slope of  $-E/R$ . Using the Coats–Redfern integral equation (referred to as C-R), Eq. (11) is obtained:

$$\ln\left[\frac{g(\alpha)}{T^2}\right] = \ln\left(\frac{AR}{\beta E}\right) - \frac{E}{RT} \quad (11)$$

where  $g(\alpha)$  is the integral function, and when  $\ln [g(\alpha)/T^2]$  is linearly related to  $1/T$ , we obtain  $E$  from the slope of  $-E/R$ . The most probabilistic function is deduced by  $Z(\alpha)-\alpha$  method, and the data obtained by  $\alpha$ ,  $f(\alpha)$ ,  $g(\alpha)$  are substituted into Eq. (12):

$$Z(\alpha) = f(\alpha)g(\alpha) \quad (12)$$

By plotting the  $Z(\alpha)-\alpha$  relationship curve, which is the standard curve; the activation energy ( $E$ ) value, the experimental data  $\beta$ ,  $\alpha$ ,  $T$ ,  $d\alpha/dt$  and F–W–O method are substituted into Eq. (13). The  $Z(\alpha)-\alpha$  curve is obtained, and the curve is the experimental curve:

$$Z(\alpha) = \left[\frac{RT^2}{\beta E}\right] \left(\frac{d\alpha}{dt}\right) \quad (13)$$

If the resulting experimental curve from Eq. (13) overlaps with the standard curve from Eq. (12), or the experimental data points all fall on a standard curve, the  $f(\alpha)$  and  $g(\alpha)$  corresponding to the standard curve are the most likely mechanistic functions [37].

## Results and discussion

### TG–IR analysis

Thermal degradation of the composite membrane: The 20%ILs-TEA-PFSA composite membrane contains a small amount of crystalline water, resulting in unexpected peaks including the peaks at 408.3 °C, 442.9 °C and 469.0 °C.

Figure 1 shows TG–IR–MS spectra of the 20%ILs-TEA-PFSA composite membrane. The TG-DTG curves are shown in Fig. 1a, where the heating rate is 20 °C min<sup>-1</sup>. Figure 1b shows the total ion chromatogram measured by TG–IR–MS, where the descending peak before 3 min is the result of injecting a small amount of air into the sample. When the retention time is 22.32 min, the relative abundance of the peak intensity is maximized. The TG–IR three-dimensional graphics and relationship between the abs-wavenumbers and time curves are shown in Fig. 1c. The time–peak intensity curve is shown in Fig. 1d, where Absorbance versus time is plotted; curve 1- $m/z=64$ , SO<sub>2</sub>; curve 2- $m/z=44$ , CO<sub>2</sub>; curve 3- $m/z=34$ , H<sub>2</sub>S, where the

sample contained a small amount of crystalline water. The figure shows that the thermal degradation of the composite membrane is mainly produced SO<sub>2</sub>, CO<sub>2</sub> and H<sub>2</sub>S gases.

TG–IR–MS analyses on the composite membranes showed that the main infrared vibration peaks are near 1300 cm<sup>-1</sup>, 1600–1700 cm<sup>-1</sup>, 2200–2600 cm<sup>-1</sup> and 3600 cm<sup>-1</sup>, which is consistent with SO<sub>2</sub>, CO<sub>2</sub> and H<sub>2</sub>S gases.

### Thermal degradation behavior

Figure 2 shows the curves of TG-DTG and the conversion rate  $\alpha$  versus time and DSC of 20% ILs/TEA/PFSA composite membrane. Figure 2a, b, respectively, represents the TG and DTG curves on the conditions of different heating rate. The onset and start temperature for thermal decomposition of the composite membrane are shown in Table 1.

Seen from the table, the  $T_{\text{start}}$ ,  $T_{\text{end}}$  and  $T_{\text{onset}}$  temperatures of the composite membrane pyrolysis are, respectively, 346.1, 570.0 and 370.7 °C when  $\beta$  is 15 °C min<sup>-1</sup>. In addition, if the conversion rate is 1.0, 5.0 and 10%, the corresponding decomposition temperatures of the membrane were 363.5, 386.1 and 399.4 °C, respectively.

Table 2 shows the nonisothermal mass loss of the composite membrane at a specific temperature. From the table, when the  $\beta$  is 15 °C min<sup>-1</sup> and the temperatures are 300, 350, 380 and 390 °C, the corresponding nonisothermal conversion  $\alpha$  of the membrane is 0, 0.32, 3.26 and 6.20%, respectively.

### Reaction time versus conversion rate $\alpha$

The conversion rate of the composite membrane versus time is shown in Fig. 2c. When the heating rates were 15, 20 and 40 °C min<sup>-1</sup>, the maximum decomposition rates  $\alpha$  of the composite membranes were 81.58, 82.27 and 79.01%, respectively, and the times to reach the reaction endpoint were 51.3 min, 38.7 min and 19.3 min, respectively. With the increased heating rate, the slope of the curve slowly increases; that is, the reaction rate of  $d\alpha/dt$  increases.

### Differential scanning calorimetry (DSC)

Since the imidazole cation exchange improves the thermal stability of the composite membrane, the DSC curves of the imidazole cation exchanging PFSA-TEA membrane in a nitrogen atmosphere were measured and are shown in Fig. 2d. Two transitions were observed in the DSC curves of the composite membrane, one distinct transition from 100 to 200 °C and another inconspicuous transition in the 350–450 °C range. The different heating rate curves all showed obvious endothermic peaks near 167.7 °C and

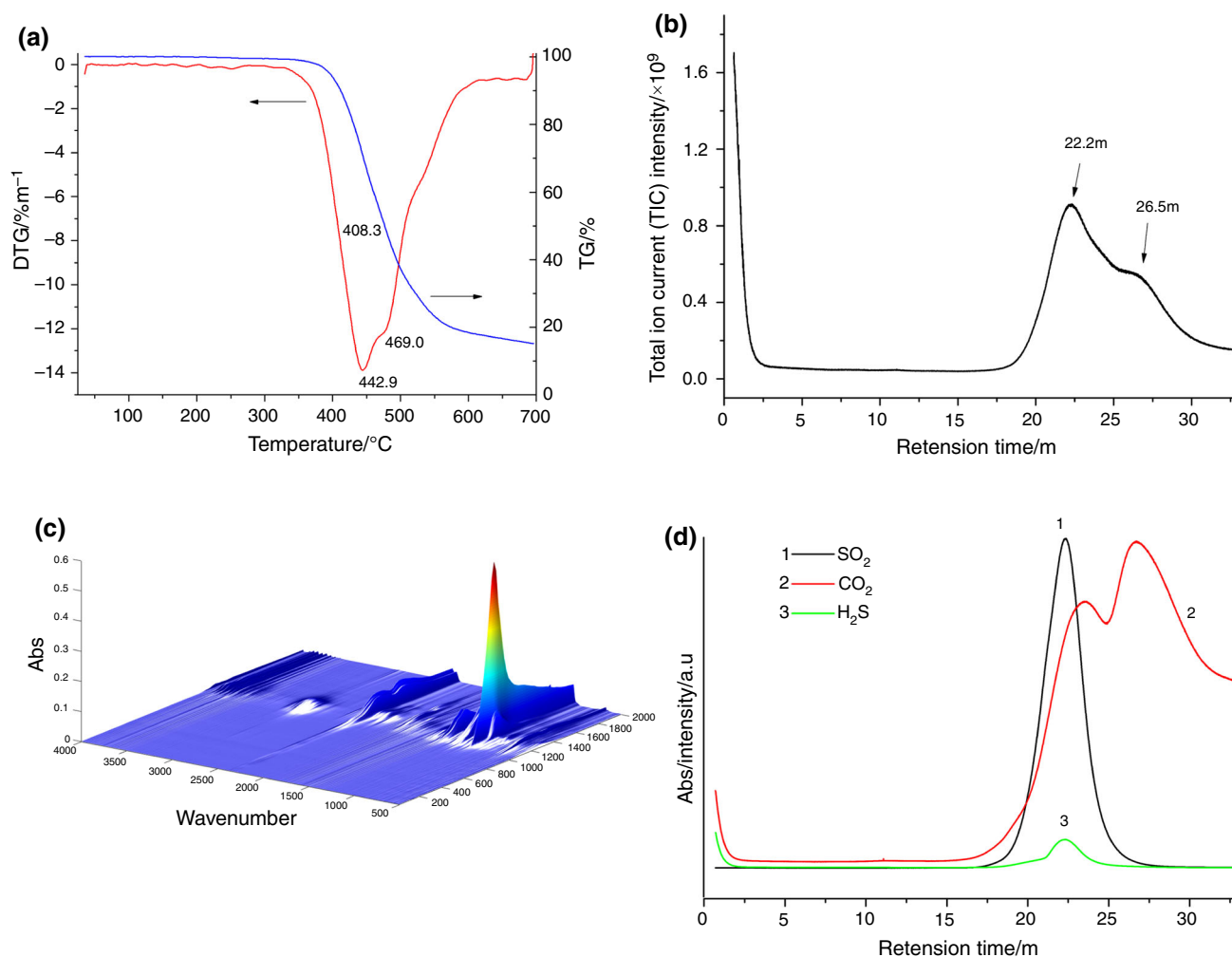


**Fig. 1** TG-IR-MS spectra of 20%ILs-TEA-PFSA composite membrane. **a** TG-DTG curves,  $\beta=20\text{ }^{\circ}\text{C min}^{-1}$ ; **b** total ion outflow; **c** TG-IR three-dimensional graphics; **d** absorbance versus time; curve 1- $m/z$

nonsignificant endothermic peaks near 396.8 °C. The former represents the evaporation and desorption of water in PFSA, and the latter corresponds to the desulfonation of the side chain of PFSA. The latter has no appreciable endothermic peak, indicating that the desulfonation is inhibited. The higher temperature corresponds to the decomposition of the PTFE skeleton. In general, the peaks corresponding to sulfuric acid and PTFE skeleton decomposition of the PFSA side chains shift to higher temperatures. The exchange of the imidazolium cations not only enhances the stability of the PFSA side chains but also enhances the PTFE main chain stability.

### Thermal decomposition kinetics

Table 3 shows the characteristic temperature of the thermal degradation of the composite membrane. It can be seen from the table that at a rate of  $15\text{ }^{\circ}\text{C min}^{-1}$ , the peak

$=64$ , SO<sub>2</sub>; curve 2- $m/z=44$ , CO<sub>2</sub>; curve 3- $m/z=34$ , H<sub>2</sub>S; sample containing a small amount of crystalline water

temperature  $T_p$  of the first, second and third stages is 398.6, 435.9 and 460.7 °C, respectively, with an increase heating rate, the peak temperature of the membrane shifted from the low- to high-temperature region.

Figure 3 shows the linear curve of membrane degradation in the first stage. The linear curve of  $\ln(\beta/T_p^2)$  and  $T_p$  is shown by Kissinger method, Eq. (6). In Fig. 3a, the slope is  $-E/R$  and the intercept is  $\ln(AR/E)$ . The kinetic parameters of the composite membrane thermal degradation as obtained by the Kissinger method are shown in Table 4.

It can be seen from table that the linear coefficient ( $r$ ) of the membrane pyrolysis are 0.9944, 0.9999 and 0.998, respectively, in the first, second and third decomposition stages, and the linear relationship is improved. The corresponding activation energies ( $E_a$ ) are 136.5, 170.8 and 159.8 kJ mol<sup>-1</sup>, respectively.

In (b) Fig. 3b, according to the linear curve of  $\lg\beta$  versus  $1/T$ , based on the Flynn-Wall-Ozawa method in Eq. (7),

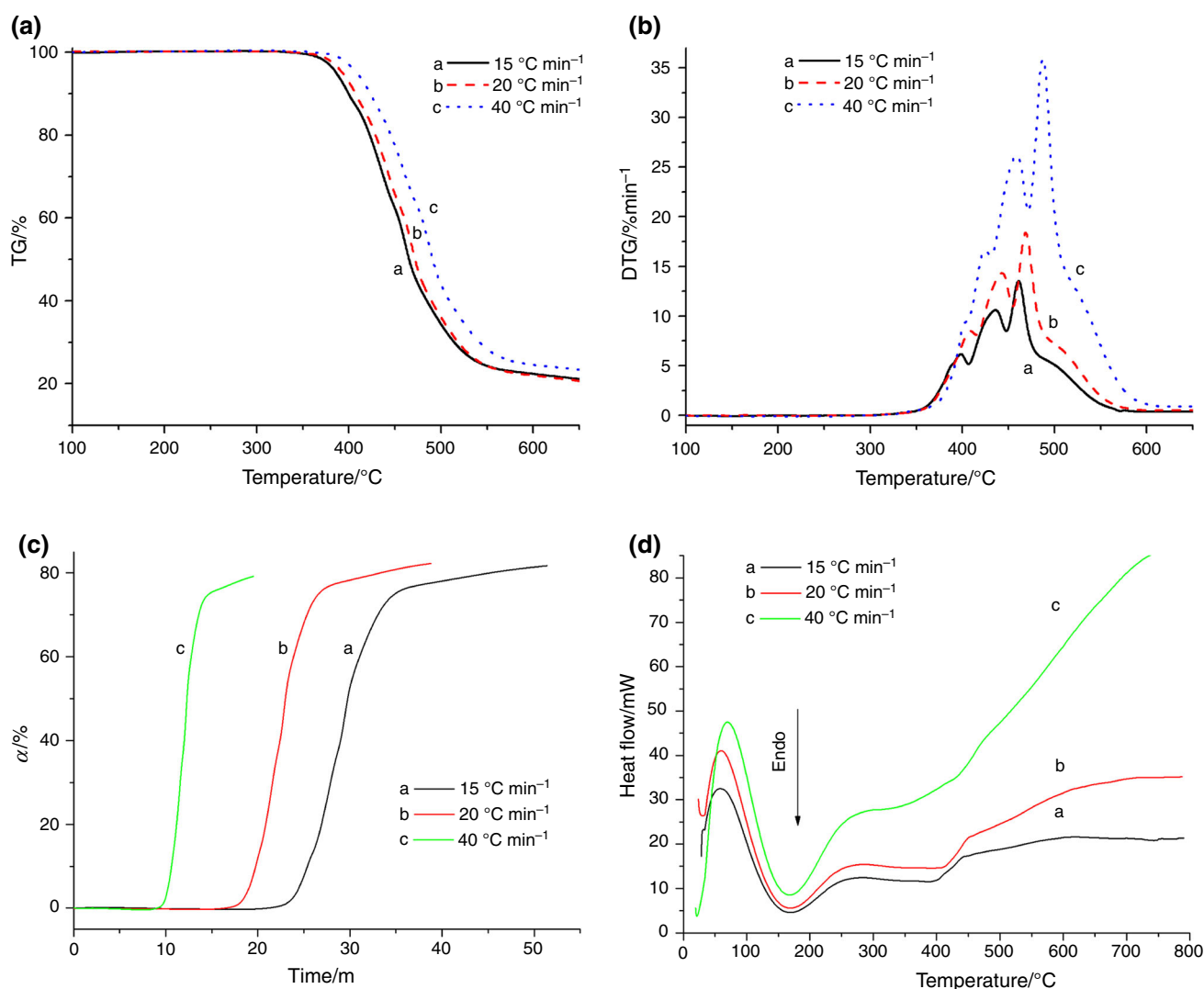


**Fig. 2** TG-DTG curve of composite membrane. **a** TG curves, **b** DTG curves, **c** conversion rate  $\alpha$  versus time, **d** DSC curves

**Table 1** Onset and start temperature for thermal decomposition of composite membrane

$\beta/^\circ\text{C min}^{-1}$	$T_{\text{start}}/^\circ\text{C}$	$T_{\text{end}}/^\circ\text{C}$	$T_{\text{onset}}/^\circ\text{C}$	$T_{0.01}/^\circ\text{C}$	$T_{0.05}/^\circ\text{C}$	$T_{0.10}/^\circ\text{C}$	$T_{0.20}/^\circ\text{C}$
15	346.1	570.0	370.7	363.5	386.1	399.4	412.7
20	353.0	598.9	380.3	370.2	392.8	407.2	428.8
40	371.4	615.6	395.5	386.4	408.4	423.4	446.1

$T_{\text{start}}$  start decomposition temperature;  $T_{\text{end}}$  termination decomposition temperature;  $T_{\text{onset}}$  starting decomposition temperature;  $T_{0.01}$  temperature at decomposition of 1%;  $T_{0.05}$  temperature at 5% decomposition;  $T_{0.10}$  temperature at 10% conversion rate;  $T_{0.20}$  temperature at 20% conversion rate)

with  $\alpha$  in the range of 0–0.10 in the first stage, the apparent measured activation energy ( $E_a$ ) is between 145.6 and 162.2 kJ mol<sup>-1</sup>, the average value of  $E$  is 155.5 kJ mol<sup>-1</sup>, and the linear coefficient ( $r$ ) is 0.9998.

Figure 3c shows a linear curve of  $\ln(\beta/T^{1.8})$  versus  $1/T$ , according to Eq. (8) using the Starink method, the apparent activation energy obtained is between 143.4 and

160.6 kJ mol<sup>-1</sup>, the average  $E_a$  is 153.5 kJ mol<sup>-1</sup>, and the linear coefficient ( $r$ ) is 0.9997.

Figure 3d shows a linear curve of  $\ln(da/dt)$  versus  $1/T$ . The Friedman method is used to determine the apparent activation energy and the obtained  $E_a$  is between 128.7 and 177.8 kJ mol<sup>-1</sup>. According to Eq. (9), the  $E_a$  value fluctuates greatly, and the average value of  $E_a$

**Table 2** Nonisothermal mass loss of the composite membrane

Temperature/°C	Conversion rate $\alpha/\%$		
	15 °C min <sup>-1</sup>	20 °C min <sup>-1</sup>	40 °C min <sup>-1</sup>
300	0	0	0
350	0.32	0.16	0
380	3.26	2.15	0.57
385	4.62	3.08	0.89
390	6.20	4.22	1.35
400	10.18	7.14	3.00

obtained is 153.5 kJ mol<sup>-1</sup>, with a linear coefficient ( $r$ ) of 0.9997.

Kinetic parameters in Tables 5–7 are obtained using the FWO method, Friedman method and starink method in first stage, according to the nonisothermal thermal gravimetry where the conversion  $\alpha$  is in the range of 0.01–0.10, 0.15–0.40, and 0.45–0.70, respectively. In the first stage, the activation energy of the three methods is similar to that of the Kissinger method, and the  $E_a$  value is approximately 20 kJ mol<sup>-1</sup> higher than 136 kJ mol<sup>-1</sup>.

Figure 4a–c shows linear curves corresponding to the membrane pyrolysis using the FWO method, starink method and Friedman method in the second stage, where  $\alpha$  is in the range of 0.15–0.40. The kinetic parameters solved by various methods in the second stage are shown in Table 6. The apparent activation energy  $E_a$  of the FWO method is between 164.0 and 168.5 kJ mol<sup>-1</sup>, the variation range is small, and the average value of  $E_a$  is 166.7 kJ mol<sup>-1</sup>, and the linear coefficient ( $r$ ) is 0.9996. The calculated  $E_a$  value is 161.6–166.6 kJ mol<sup>-1</sup> by the Starink method, and the average value of  $E_a$  is 164.6 kJ mol<sup>-1</sup> with a linear coefficient ( $r$ ) of 0.9996. The  $E_a$  solved by the Friedman method is in the range of 149.7–174.7 kJ mol<sup>-1</sup>. Compared to the Starink method, the Flynn–Wall–Ozawa method has a larger  $E_a$  value, and the average value of  $E_a$  is 164.1 kJ mol<sup>-1</sup>, with a linear coefficient ( $r$ ) of 0.9984. In the second decomposition stage, the difference in activation energy between the three methods is small, and the activation energy in the second stage is 170.8 kJ mol<sup>-1</sup>, which is similar than that of the Kissinger method,

indicating that the resulting activation energy error is small in this decomposition stage with the adopted four methods. Figure 4d–f shows the linear curves of membrane pyrolysis in the third stage, and  $\alpha$  is in the range of 0.45–0.70, using the FWO method, Starink method and Friedman method. The kinetic parameters solved by various methods in the third stage are shown in Table 7. The apparent activation energy ( $E_a$ ) of the FWO method is between 167.3 and 182.4 kJ mol<sup>-1</sup>, and the average value of  $E_a$  is 174.3 kJ mol<sup>-1</sup> with a linear coefficient ( $r$ ) of 0.9963.

The  $E_a$  value of the Starink method is between 164.8 and 180.2 kJ mol<sup>-1</sup>, the average value of  $E_a$  is 171.8 kJ mol<sup>-1</sup>, and the linear coefficient ( $r$ ) is 0.9948. The  $E_a$  calculated by the Friedman method is between 140.7 and 198.7 kJ mol<sup>-1</sup>, and its  $E_a$  value fluctuates greatly compared to Flynn–Wall–Ozawa method and Starink method. The average value of  $E_a$  is 174.5 kJ mol<sup>-1</sup>, and the linear coefficient ( $r$ ) is 0.9874. In the third stage, the difference in activation energy between the three methods is small, while the Kissinger method has an  $E_a$  value of 159.7 kJ mol<sup>-1</sup>, which is 13 kJ mol<sup>-1</sup> smaller than that calculated with the other three methods.

Figure 5 shows the relationship between the apparent activation energy  $E_a$  of thermal degradation of the composite membrane with the decomposition rate ( $a$ ). It can be seen from the figure that when  $\alpha$  is in the range of 0–0.1, the activation energy  $E_a$  increases slowly to 160 kJ mol<sup>-1</sup>. With an increased decomposition rate ( $a$ ), the  $E_a$  value fluctuates less. When  $\alpha$  is 0.6, the  $E_a$  value reached a maximum of 182.4 kJ mol<sup>-1</sup>. With  $\alpha$  in the range of 0.01–0.70, the  $E_a$  value is between 145 and 180 kJ mol<sup>-1</sup>. The  $E_a$  value calculated by the Starink method is very close to that of the FWO method, but the  $E_a$  value is smaller than the FWO method.

The  $E_a$  value solved by the Friedman method fluctuates significantly with the increase in the decomposition rate ( $a$ ), when  $\alpha$  is 0.05, the  $E_a$  value is the smallest, which is 128.7 kJ mol<sup>-1</sup>, and when  $\alpha$  is 0.55, the maximum value of  $E_a$  is achieved at 198.7 kJ mol<sup>-1</sup>. Table 8 shows the kinetic parameters for the thermal degradation of the membrane obtained by different methods. As seen in Table 8, when  $\alpha$  is 0.01–0.1, 0.15–0.40 and 0.45–0.70, the average apparent activation energy  $E_a$  of membrane pyrolysis in the first,

**Table 3** Characteristic temperature of thermal degradation

Stage	15 °C min <sup>-1</sup>		20 °C min <sup>-1</sup>		40 °C min <sup>-1</sup>	
	$T_p/^\circ\text{C}$	$d\alpha/dt \text{ \%min}^{-1}$	$T_p/^\circ\text{C}$	$d\alpha/dt \text{ \%min}^{-1}$	$T_p/^\circ\text{C}$	$d\alpha/dt \text{ \%min}^{-1}$
1st	398.6	6.07	408.3	8.31	424.8	16.66
2nd	435.9	10.55	442.9	14.42	459.1	26.19
3rd	460.7	13.36	468.7	18.29	487.3	36.07

$T_p$  peak temperature,  $d\alpha/dt$  differential decomposition rate



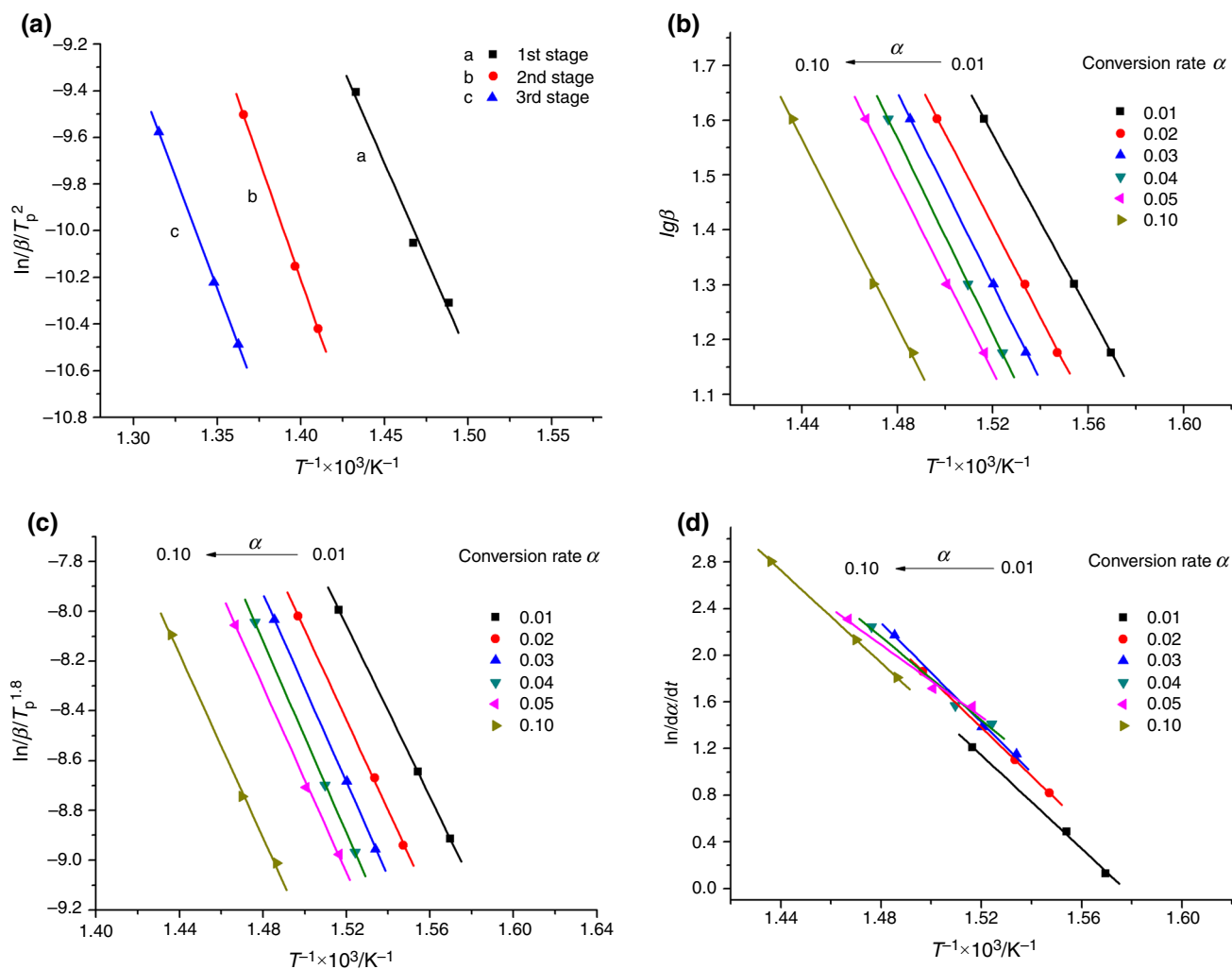


**Fig. 3** Linear curves of composite membrane degradation in different methods (1st stage). **a**  $\ln(\beta/T_p^2)$  versus  $1/T_p$ , **b**  $\lg \beta$  versus  $1/T$ , **c**  $\ln(\beta/T_p^{1.8})$  versus  $1/T$ , **d**  $\ln(da/dt)$  versus  $1/T$

**Table 4** Kinetic parameters of thermal degradation obtained by Kissinger method

Stage	$E/\text{kJ mol}^{-1}$	$A/\text{min}^{-1}$	$r$	SD
1st	136.5	$2.26 \times 10^{10}$	0.9944	0.06981
2nd	170.8	$2.41 \times 10^{12}$	0.9998	0.01245
3rd	159.8	$1.27 \times 10^{11}$	0.9998	0.01279

$E$  apparent activation energy/ $\text{kJ mol}^{-1}$ ,  $r$  linear coefficient, SD standard deviation

second and third stages obtained by various methods are 151.3, 166.5 and 170.1  $\text{kJ mol}^{-1}$ , respectively.

### Thermal degradation mechanism

Based on the linear curves obtained by the A-B-S and C-R methods, the  $\ln[da/f(\alpha)dT]$  and  $\ln[g(\alpha)/T^2]$  were linearly

fitted to  $1/T$ . The apparent activation energy  $E_a$  calculated from the A-B-S differential method is 144.93  $\text{kJ mol}^{-1}$ , with a linear coefficient of 0.9810, and a standard deviation (SD) of 0.0921. The  $E_a$  obtained by the C-R integral method of Eq. (12) was 144.9  $\text{kJ mol}^{-1}$ , the linear coefficient was 0.9903, and the SD was 0.06019. It can be seen that the  $E_a$  of membrane pyrolysis is close in these two methods.

In addition, the basic data obtained from the TG-DTG curves of the composite membrane and the common 41 types of thermal decomposition mechanism functions [37] and their  $f(\alpha)$  and  $g(\alpha)$  are, respectively, introduced into Eqs. (13) and (14). When the heating rate  $\beta$  is 20  $^\circ\text{C min}^{-1}$ , the  $Z(\alpha)$ - $\alpha$  standard curve versus the experimental curve is shown in Fig. 6, it can be seen from the figure that when  $\alpha$  is in the range of 0.01–0.10, the experimental curves of  $Z(\alpha)$ - $\alpha$  almost overlap with the standard curve. The  $E_a$ -values solved by the A-B-S method and the C-R method

**Table 5** Kinetic parameters of thermal degradation obtained by various methods (1st stage)

$\alpha$	FWO method			Starink method			Friedman method		
	$r$	SD	$E$	$r$	SD	$E$	$r$	SD	$E$
0.01	1.0000	0.00007	145.6	1.0000	0.00173	143.4	0.9997	0.03533	166.8
0.02	0.9997	0.00761	153.1	0.9997	0.01762	151.1	1.0000	0.00119	172.2
0.03	0.9999	0.00413	159.3	0.9999	0.00960	157.5	0.9984	0.04269	177.8
0.04	0.9999	0.00308	162.2	0.9999	0.00697	160.6	0.9929	0.07468	148.8
0.05	0.9997	0.00801	157.4	0.9996	0.01834	155.4	0.9930	0.06590	128.7
0.10	0.9993	0.01137	155.3	0.9993	0.02594	153.1	1.0000	0.00187	164.7
Mean			155.5			153.5			159.8

$\alpha$  conversion rate,  $r$  linear coefficient,  $SD$  standard deviation,  $E$  apparent activation energy/kJ mol<sup>-1</sup>

are close, and the  $E_a$  value data happens to be within the  $Z$  ( $\alpha$ )– $\alpha$  overlap range This indicates that the reaction sequence of No.35 ( $n=4$ ) and its thermal decomposition mechanism of 20% ILs/TEA/PFSA composite membrane follows the differential mechanism function  $f(\alpha)$  of  $1-(1-\alpha)^4$ , and the integral mechanism function  $g(\alpha)$  is  $1/4(1-\alpha)^{-3}$ . It can be inferred that the obtained differential and integral mechanics functions  $f(a)$  and  $g(a)$  are the mechanistic functions of the interval.

### Isothermal lifetime

The isothermal mass-loss curves of the 20%[BMIM]BF<sub>4</sub>/TEA/PFSA composite membrane are shown in Fig. 7.

The conversion rate of composite membrane changed with reaction time at 410, 415 and 420 °C and is demonstrated in Fig. 7a, which shows the isothermal curves of  $\alpha$  versus  $t_a$ . The curves  $\lg t_a$  versus  $T^{-1}$  are shown in Fig. 7b, and the reacted fraction  $\alpha$  of composite membrane was 10 and 15%. As seen from the figure, the two lines formed a stronger linear relationship Conversion rate curves were measured at 683.15, 688.15 and 693.15 K at a constant temperature ( $T_0$ ), with a mass loss of 10 and 15% corresponding to the time  $t_a$  required, and the experimental data and lifetimes of the composite membrane at different temperatures are shown in Table 9. In the case of a one-step decomposition process of the composite membrane under isothermal conditions (constant temperature,  $T_0$ ), the time to reach  $\alpha$  given degree of conversion can be determined by the following equation [38]:

$$t_a = \frac{g(\alpha)}{\left[ A \exp\left(-\frac{E_a}{RT_0}\right) \right]} \quad (14)$$

where  $t_a$  is the time/min required for the conversion rate of  $\alpha$ ,  $T_0$  is the isothermal absolute temperature/K,  $R$  is the gas constant/J mol<sup>-1</sup> K<sup>-1</sup>,  $A$  is the pre-exponential factor/min<sup>-1</sup>,  $E_a$  is the activation energy/kJ mol<sup>-1</sup>, and  $g(\alpha)$  is the integral mechanism function. Equation (14) can be used to

predict the lifetime of material under isothermal conditions at a temperature  $T_0$ . Assuming that the decomposition process obeys first-order kinetics:  $t_{5\%}$ ,  $t_{10\%}$  and  $t_{15\%}$  were the time/min for a mass loss of 5, 10 and 15%, respectively.

$$g(\alpha) = -\ln(1 - \alpha) \quad (15)$$

Substituted  $g(\alpha)$  into Eqs. (14) and (15) yields the following Eq. (16):

$$t_a = \frac{-\ln(1 - \alpha)}{\left[ A \exp\left(-\frac{E_a}{RT_0}\right) \right]} \quad (16)$$

On both sides of the logarithm, the following Eq. (17) is obtained:

$$\ln t_a = \ln[-\ln(1 - \alpha)] - \ln A + \frac{E_a}{RT_0} \quad (17)$$

When  $\alpha$  is defined,  $E_a$  and  $A$  are constant, For a conversion rate of 10%,  $\ln t_a$  and  $T_0^{-1}$  are plotted to form a straight line if a linear relationship formed, then the  $A$  and  $E_a$  can be calculated by the slope and the intercept and according to Table 9, where the slope is  $8.710 \times 10^3$  and the intercept is  $-11.4588$ , the linear coefficient ( $r$ ) is 0.9992, SD is 0.00522; then  $E_a=166.8$  kJ mol<sup>-1</sup>,  $A=3.05 \times 10^{10}$  min<sup>-1</sup>. If the constant temperature operation at  $T_0=180$  °C,  $\alpha=5\%$  and  $\alpha=10\%$ , according to Eq. (16), the thermal lifetimes  $t_{5\%}$  and  $t_{10\%}$  of the composite membrane are  $4.83 \times 10^5$  and  $9.83 \times 10^5$  h, respectively. The obtained isothermal thermal lifetimes are shown in Table 10 based on Eq. (16).

### Master plots based on the differential form of the generalized kinetic equation

Using the experimental data from the isothermal mass-loss trace for the thermal decomposition of 20%[BMIM]BF<sub>4</sub>/TEA/PFSA composite membrane under a nitrogen atmosphere, the practical usefulness of the master plots was examined. Figure 8 shows the kinetic curves for the thermal decomposition of the composite membrane obtained

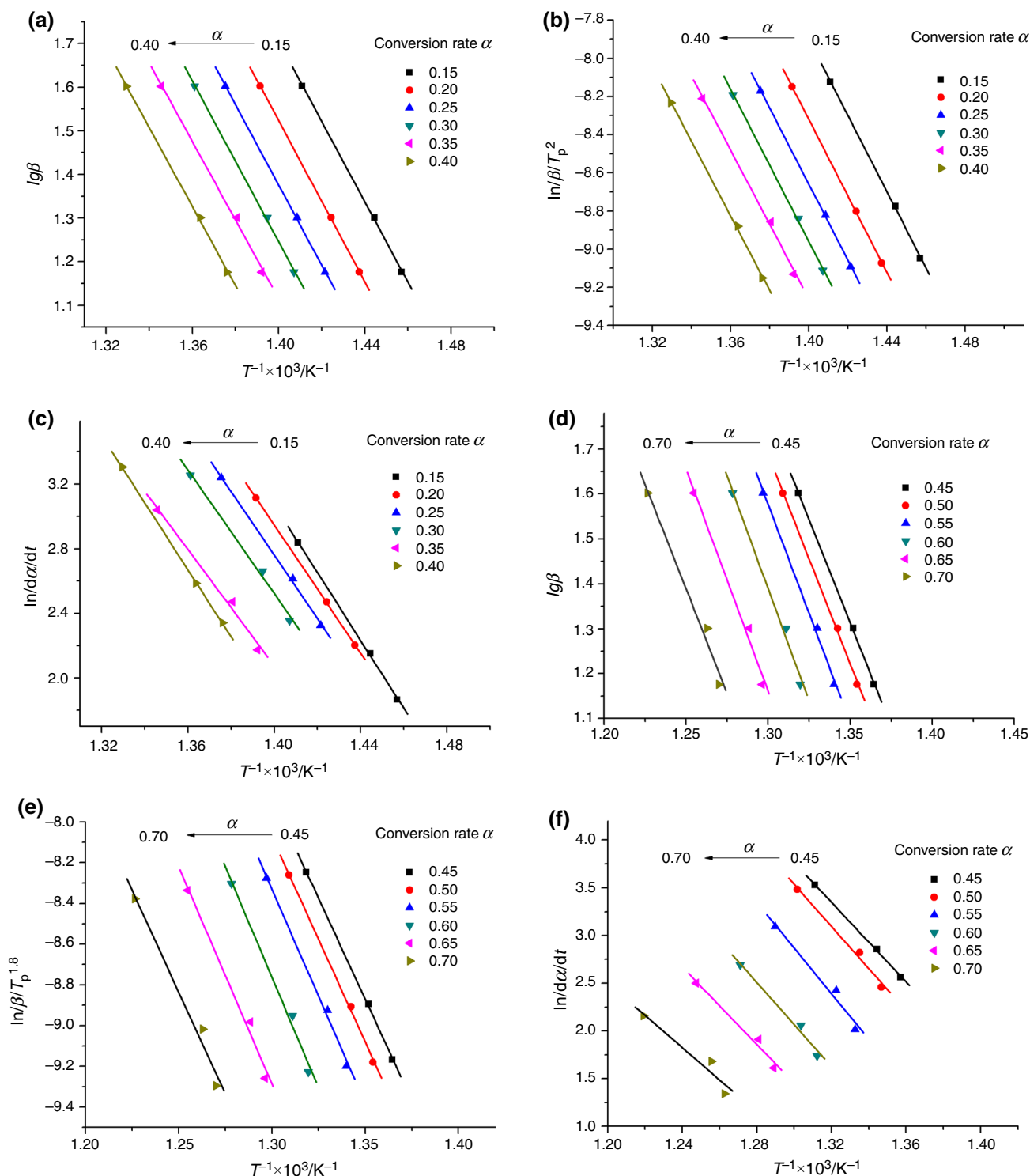


**Fig. 4** Linear curves of composite membrane obtained by different methods. **a**  $\lg \beta$  versus  $1/T$  (2nd stage), **b**  $\ln(\beta/T_p^{1.8})$  versus  $1/T$  (2nd stage), **c**  $\ln(d\alpha/dt)$  versus  $1/T$  (2nd stage), **d**  $\lg \beta$  versus  $1/T$  (3rd stage), **e**  $\ln(\beta/T_p^{1.8})$  versus  $1/T$  (3rd stage), **f**  $\ln(d\alpha/dt)$  versus  $1/T$  (3rd stage)

from the isothermal mass-loss measurements at 688 K. Using a reference point at  $\alpha=0.5$ , Eqs. (18) and (19) can be obtained according to the kinetic analysis of solid-state reactions [39]:

$$\theta = \int_0^t \exp\left(-\frac{E}{RT}\right) dt \quad (18)$$

**Table 6** Kinetic parameters of thermal degradation obtained by various methods (2nd stage)

$\alpha$	FWO method			Starink method			Friedman method		
	$r$	$SD$	$E$	$r$	$SD$	$E$	$r$	$SD$	$E$
0.15	0.9998	0.00643	167.7	0.9997	0.01507	165.9	0.9998	0.01521	174.7
0.20	0.9999	0.00300	168.5	0.9999	0.00707	166.6	1.0000	0.00603	164.8
0.25	0.9999	0.00485	167.7	0.9999	0.01128	165.6	0.9992	0.02728	163.4
0.30	0.9997	0.00787	167.5	0.9996	0.01830	165.3	0.9971	0.04959	159.2
0.35	0.9988	0.01539	164.0	0.9986	0.03556	161.6	0.9945	0.06505	149.7
0.40	0.9996	0.00900	165.0	0.9995	0.02082	162.4	0.9999	0.00917	172.7
Mean			166.7			164.6			164.1

$\alpha$  conversion rate,  $r$  linear coefficient,  $SD$  standard deviation,  $E$  apparent activation energy/kJ mol<sup>-1</sup>

**Table 7** Kinetic parameters of thermal degradation obtained by different methods (3rd stage)

$\alpha$	FWO method			Starink method			Friedman method		
	$r$	$SD$	$E$	$r$	$SD$	$E$	$r$	$SD$	$E$
0.45	0.9998	0.00597	167.3	0.9998	0.01386	164.8	0.9996	0.02088	172.9
0.50	0.9994	0.01098	169.9	0.9993	0.02538	167.4	0.9948	0.07474	183.3
0.55	0.9980	0.01950	176.9	0.9977	0.04508	174.7	0.9877	0.12055	198.7
0.60	0.9959	0.02805	182.4	0.9953	0.06463	180.2	0.9907	0.09287	182.9
0.65	0.9943	0.03314	179.9	0.9934	0.07654	177.4	0.9883	0.09717	168.3
0.70	0.9904	0.04272	169.6	0.9890	0.09841	166.4	0.9619	0.15826	140.7
Mean			174.3			171.8			174.5

$\alpha$  conversion rate,  $r$  linear coefficient,  $SD$  standard deviation,  $E$  apparent activation energy/kJ mol<sup>-1</sup>

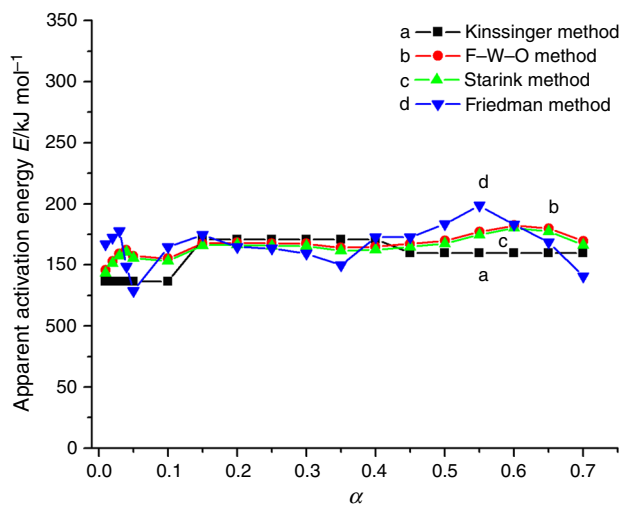


**Fig. 5** Apparent activation energy  $E$  of composite membrane pyrolysis with conversion rate  $\alpha$

$$\frac{d\alpha/d\theta}{(d\alpha/d\theta)_{\alpha=0.5}} = \frac{f(\alpha)}{f(0.5)} \tag{19}$$

where  $\theta$  is a generalized time that denotes the reaction time taken to attain a particular  $\alpha$  at infinite temperature,  $d\alpha/d\theta$

corresponds to the generalized reaction rate,  $f(\alpha)$  is a differential mechanism function, and  $f(0.5)$  is a constant for a given kinetic model function. Based on Eq. (20), it is assumed that the decomposition process follows the first-order reaction kinetics. Figure 8 compares the theoretical master plots of  $f(\alpha)/f(0.5)$  against  $\alpha$  with the experimental master plots of  $(d\alpha/d\theta)/(d\alpha/d\theta)_{\alpha=0.5}$  versus  $\alpha$  calculated from the experimental data for the thermal decomposition of the 20%[BMIM]BF<sub>4</sub>/TEA/PFSA composite membrane. Because the exponential terms in Eq. (20) can be neglected for the isothermal kinetic data, and the experimental master plot for the isothermal kinetic data was obtained as  $(d\alpha/d\theta)/(d\alpha/d\theta)_{\alpha=0.5}$  against  $\alpha$ . When  $\alpha=0.2-0.4$ , it is clearly seen from figure that the experimental master plots are in good agreement with the theoretical master plot corresponding to the F1 mechanism, irrespective of the temperature profiles of the kinetic data, and its mechanism function,  $f(\alpha)=(1-\alpha)$ ,  $g(\alpha)=-\ln(1-\alpha)$ .

$$\frac{d\alpha/d\theta}{(d\alpha/d\theta)_{\alpha=0.5}} = \frac{d\alpha/dt}{(d\alpha/dt)_{\alpha=0.5}} \frac{\exp(E/RT)}{\exp(E/RT_{0.5})} \tag{20}$$

**Table 8** Kinetic parameters of thermal degradation obtained by various methods

Method	$E/\text{kJ mol}^{-1}$	$r$	Stage	Method	$E/\text{kJ mol}^{-1}$	$r$	Stage	Method	$E/\text{kJ mol}^{-1}$	$r$	Stage
Kissinger	136.5	0.9944	1st	Kissinger	170.8	0.9998	2nd	Kissinger	159.8	0.9998	3rd
FWO	155.5			FWO	166.7			FWO	174.3		
Starink	153.5			Starink	164.6			Starink	171.8		
Friedman	159.8			Friedman	164.1			Friedman	174.5		
Mean	151.3			Mean	166.5			Mean	170.1		

$r$  linear coefficient,  $E$  apparent activation energy/ $\text{kJ mol}^{-1}$

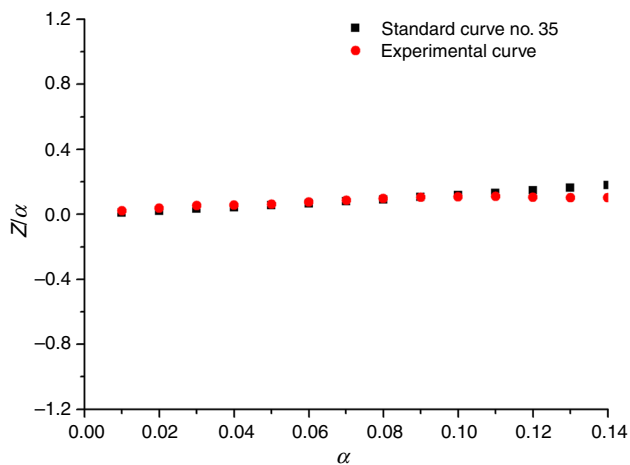


**Fig. 6**  $Z(\alpha)$ - $\alpha$  standard curve and experimental curve.  $\beta=20\text{ }^{\circ}\text{C min}^{-1}$ ,  $\alpha$  0.01-0.10

### Master plots based on the integral form of the kinetic data

$$\frac{g(\alpha)}{g(0.5)} = \frac{\theta}{\theta_{0.5}} \quad (21)$$

$$g(\alpha) = \int_0^{\alpha} \frac{d\alpha}{f(\alpha)} = A \int_0^{\theta} d\theta = A\theta \quad (22)$$

where  $g(\alpha)$  is the integral mechanism function, because the exponential term in Eq. (22) is a constant during the course of the reaction, the value of  $\theta/\theta_{0.5}$  at a given  $\alpha$  is equivalent to  $t/t_{0.5}$ . Equation (21) is then transformed into:

$$\frac{g(\alpha)}{g(0.5)} = \frac{t}{t_{0.5}} \quad (23)$$

Based on Eqs. (21), (22) and (23), the experimental master plots of  $\theta/\theta_{0.5}$  against  $\alpha$  constructed from the experimental isothermal data of the composite membrane compared with the theoretical master curves of  $g(\alpha)/g(0.5)$

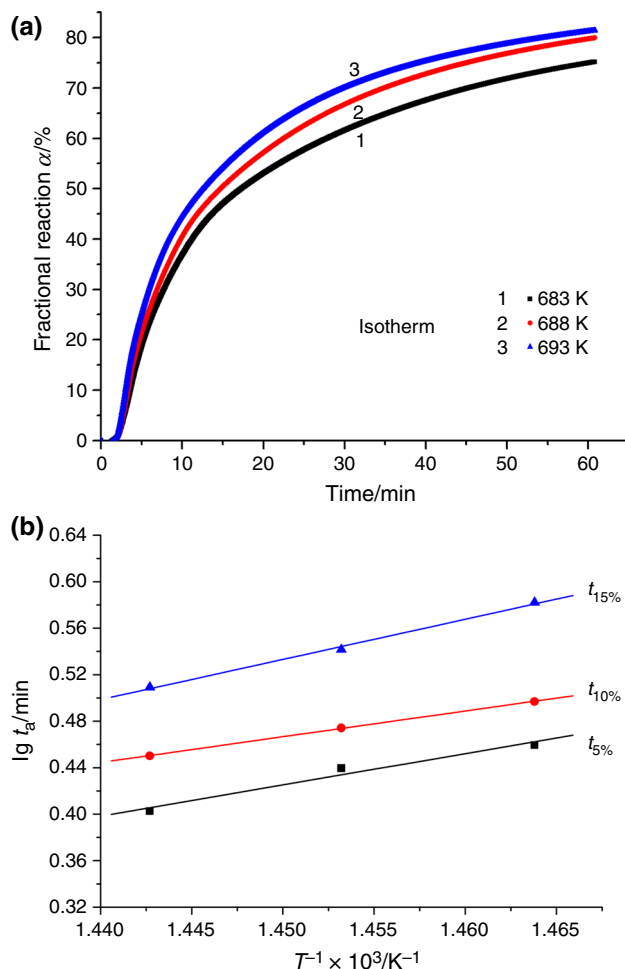


**Fig. 7** Isothermal mass-loss trace curves for the composite membrane: **a** Isothermal curves  $\alpha$  versus  $t_a$ ; **b** curves of  $\lg t_a$  versus  $T^{-1}$  when conversion rate  $\alpha$  was 10 and 15%, respectively

against  $\alpha$  are shown in Fig. 9. The master plot for the isothermal mass loss is calculated using Eq. (23) as  $t/t_{0.5}$  against  $\alpha$ . The experimental master plots obtained for the thermal decomposition of the 20% [BMIM]BF<sub>4</sub>/TEA/PFSA composite membrane are compared in the same figure, with the theoretical master plot corresponding to the F1 kinetic

**Table 9** Lifetime of composite membrane in different temperature

T/K	$t_{5\%}/\text{min}$	$t_{10\%}/\text{min}$	$t_{15\%}/\text{min}$
683.15	2.52	3.63	4.38
688.15	2.75	3.33	3.93
693.15	2.87	3.02	3.51

$t_{5\%}$ ,  $t_{10\%}$  and  $t_{15\%}$  were the time/min with mass loss of 5, 10 and 15%, respectively

**Table 10** Isothermal thermal life

T/°C	$t_{5\%}/\text{min}$	$t_{10\%}/\text{min}$	$t_{15\%}/\text{min}$
140	$2.1 \times 10^9$	$4.3 \times 10^9$	$6.7 \times 10^9$
180	$2.9 \times 10^7$	$5.9 \times 10^7$	$9.1 \times 10^7$
200	$4.4 \times 10^6$	$9.1 \times 10^6$	$1.4 \times 10^7$
240	$1.6 \times 10^5$	$3.3 \times 10^5$	$5.1 \times 10^5$
280	$9.6 \times 10^3$	$2.0 \times 10^4$	$3.0 \times 10^4$
320	$8.3 \times 10^2$	$1.7 \times 10^3$	$2.7 \times 10^3$
360	$9.8 \times 10$	$2.0 \times 10^2$	$3.1 \times 10^2$
420	6.3	13.0	20.0

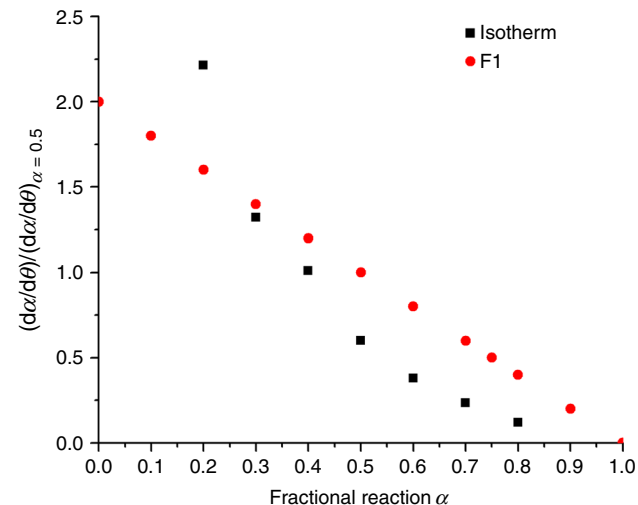


**Fig. 8** A comparison of the experimental master plots of  $(d\alpha/d\theta)/(d\alpha/d\theta)_{\alpha=0.5}$  against  $\alpha$  for the thermal decomposition of 20%[BMIM]BF<sub>4</sub>/TEA/PFSA composite membrane

model and its mechanism function  $f(\alpha)=(1-\alpha)$ ,  $g(\alpha)=-\ln(1-\alpha)$ , This indicates a close agreement, irrespective of quite different temperature programs.

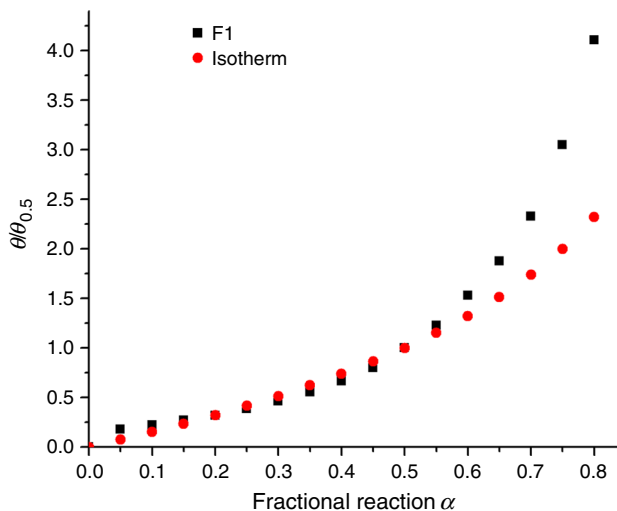


**Fig. 9** A comparison of the experimental master plots of  $\theta/\theta_{0.5}$  against  $\alpha$  for the thermal decomposition of composite membrane with the theoretical master curves of  $g(\alpha)/g(0.5)$  against  $\alpha$

**Master plots based on both the integral and differential forms of the kinetic equation  $\theta$**

$$\theta \frac{d\alpha}{d\theta} = f(\alpha)g(\alpha) \tag{24}$$

$$\frac{\theta(d\alpha/d\theta)}{\theta_{0.5}(d\alpha/d\theta)_{\alpha=0.5}} = \frac{f(\alpha)g(\alpha)}{f(0.5)g(0.5)} \tag{25}$$

According to Eqs. (24) and (25), the experimental differential master plots  $\theta d\alpha/d\theta$  against  $\alpha$  for the thermal

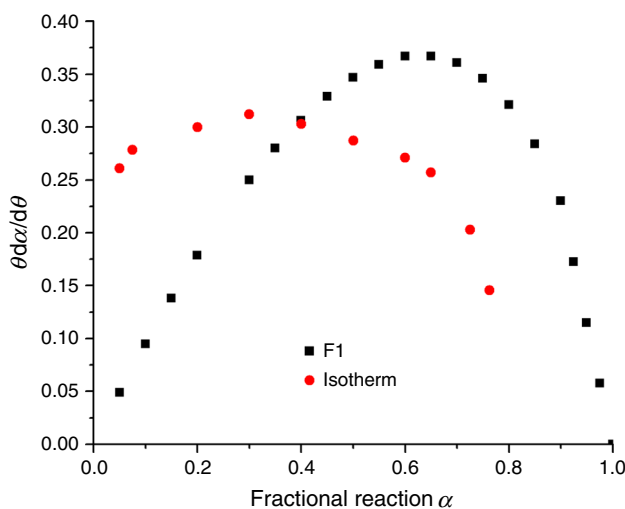


**Fig. 10** A comparison of the experimental master plots of  $\theta(d\alpha/d\theta)$  against  $\alpha$  for the thermal decomposition of composite membrane with the theoretical master curves of  $f(\alpha)g(\alpha)$  against  $\alpha$

decomposition of the composite membrane compared with the theoretical master curves of  $f(\alpha)g(\alpha)$  against  $\alpha$  are shown in Fig. 10 and were obtained by multiplying the values of  $(d\alpha/d\theta)$  and  $\theta$  at a given  $\alpha$ . The experimental master plots for the isothermal data fit well with the theoretical curve of  $f(\alpha)g(\alpha)$  against  $\alpha$  corresponding to an F1 kinetic model, but the former curve is slightly shifted to the left.

The perfluorosulfonic acid (PFSA) proton membrane reacted with triethylamine (TEA), and a 20% [BMIM]BF<sub>4</sub>/TEA/PFSA composite membrane was prepared by doping the ionic liquid [BMIM] BF<sub>4</sub>. The kinetic parameters of the membrane thermal degradation was obtained. The results show that when the heating rate  $\beta$  is 15, 20 and 40 °C min<sup>-1</sup>, using a nonisothermal nonmodel method, the thermal decomposition of the composite membrane undergoes three stages. The conversion rate  $\alpha$  of the three stages is in the range of 0.01–0.10, 0.15–0.40 and 0.45–0.70, respectively. The average apparent activation energies  $E_a$  in the first, second and third stages of membrane pyrolysis were 151.3, 166.5 and 170.1 kJ mol<sup>-1</sup>, respectively. If the heating rate  $\beta$  is 15 °C mol<sup>-1</sup>, the temperature at which 1% of the composite membrane decomposed is 363.5 °C. Identically, if heated to 350 °C, the conversion rate of the composite membrane is 0.32%. If the heating rate  $\beta$  equals 20 °C min<sup>-1</sup>, the thermal degradation process of the composite membrane follows the chemical reaction order ( $n=4$ ), and the mechanistic function  $f(\alpha)$  is  $1-(1-\alpha)^4$  and  $g(\alpha)$  is  $1/4(1-\alpha)^{-3}$ .

## Conclusions

A 20% [BMIM]BF<sub>4</sub>/TEA/PFSA composite membrane was prepared by doping the ionic liquid [BMIM] BF<sub>4</sub> with perfluorosulfonic acid (PFSA), which was first neutralized with triethylamine (TEA). The kinetic parameters of membrane thermal degradation were obtained using nonisothermal nonmodel methods. The results show that when the heating rate  $\beta$  is 15, 20 and 40 °C min<sup>-1</sup>, the thermal decomposition of the composite membrane undergoes three stages, and the conversion rate  $\alpha$  of the three stages is in the range of 0.01–0.10, 0.15–0.40 and 0.45–0.70.

The average apparent activation energies  $E_a$  in the first, second and third stages of membrane pyrolysis were 151.3, 166.5 and 170.1 kJ mol<sup>-1</sup>, respectively. If the heating rate  $\beta$  is 15 °C mol<sup>-1</sup>, the temperature of the composite membrane at 1% decomposition is 363.5 °C, and if heated to 350 °C, the conversion rate of the membrane is 0.32%.

It can be seen that the composite membrane is stable at 350 °C when  $\beta$  is 15 °C min<sup>-1</sup> and If the decomposition process follows isothermal first-order reaction and the conversion rate  $\alpha$  is 10%, the activation energy  $E_a$  of the

composite membrane is 166.8 kJ mol<sup>-1</sup>. If heated at 180 °C to a mass loss of 5% and 10%, the corresponding thermal life  $t_{5\%}$  and  $t_{10\%}$  of the composite membrane would be  $4.83 \times 10^5$  and  $9.83 \times 10^5$  h, respectively. If the heating rate  $\beta$  is 20 °C min<sup>-1</sup>, the thermal degradation process of the composite membrane follows the chemical reaction order ( $n=4$ ), the mechanism function  $f(\alpha)$  is  $1-(1-\alpha)^4$  and  $g(\alpha)$  is  $1/4(1-\alpha)^{-3}$ .

In addition, using the isothermal data from the 20% [BMIM]BF<sub>4</sub>/TEA/PFSA composite membrane at 688 K, assuming a first-order reaction, the theoretical master curve was compared with the experimental master plots of the  $d\alpha/d\theta/(d\alpha/d\theta)_{\alpha=0.5}$  versus  $\alpha$ . The  $\theta/\theta_{0.5}$  versus  $\alpha$  and the  $(d\alpha/d\theta)_0$  versus  $\alpha$  curves overlap well. TG–IR–MS analysis indicated that the main infrared vibration peaks are near 1300 cm<sup>-1</sup>, 1600–1700 cm<sup>-1</sup>, 2200–2600 cm<sup>-1</sup> and 3600 cm<sup>-1</sup> and consist of SO<sub>2</sub>, CO<sub>2</sub> and H<sub>2</sub>S gases.

**Acknowledgements** This research was financially supported by the following grants: (1) Anhui Province University Students Innovation and Entrepreneurship Program (AH201410361217), (2) Anhui International Science and Technology Cooperation Program (06088018), (3) Huainan Municipal Science and Technology Program (2011A07923).

## References

- Shi Q, Tao K, Zhang Q, Xue L, Zhang Y. Progress on application of ionic liquids in proton exchange membranes. *Membr Sci Technol.* 2013;33(3):113–20.
- Ren S, Xu Mei-ling. Process of ionic liquid based proton exchange membranes. *Chin J Power Sources.* 2014;38(2):394–7.
- Gharagheizi F, Keshavarz MH. A group contribution method for estimation of glass-transition temperature of 1, 3-dialkylimidazolium ionic liquid. *J Therm Anal Calorim.* 2013;114:1363–82.
- Che B-K, Wu T-Y, Kuo C-W, Peng Y-C. 4,4-Oxydianiline (ODA) containing sulfonated polyimide/protic ionic liquid composite membranes for anhydrous proton conduction. *Int J Hydrog Energy.* 2013;38:11321–30.
- Lee S-Y, Yasuda T, Watanabe M. Fabrication of protic ionic liquid/sulfonated polyimide composite membranes for non-humidified fuel cells. *J Power Sources.* 2010;195:5909–14.
- Kowsari E, Zare A, Ansari V. Phosphoric acid-doped ionic liquid-functionalized graphene oxide/sulfonated polyimide composites as proton exchange membrane. *Int J Hydrog Energy.* 2015;40:13964–78.
- Dahi A, Fatyeyeva K, Langevin D, Chappay C, Rogalsky SP, Tarasyuk OP, Marais S. Polyimide/ionic liquid composite membranes for fuel cells operating at high temperatures. *Electrochim Acta.* 2014;130:830–40.
- Malik RS, Verma P, Choudhary V. A study of new anhydrous, conducting membranes based on composites of aprotic ionic liquid and cross-linked SPEEK for fuel cell application. *Electrochim Acta.* 2015;152:352–9.
- Yi S, Zhang F, Li W, Huang C, Zhang H, Pana M. Anhydrous elevated-temperature polymer electrolyte membranes based on ionic liquids. *J Membr Sci.* 2011;366:349–55.
- Zhang H, Wu W, Wang J, Zhang T, Shi B, Liu J, Cao S. Enhanced anhydrous proton conductivity of polymer electrolyte

- membrane enabled by facile ionic liquid-based hopping pathways. *J Membr Sci.* 2015;476:136–47.
11. Xu Q, Zhou L, Wang J. Fabrication and characterization of phosphoric acid doped imidazolium ionic liquid polymer composite membranes. *J Mol Liq.* 2015;206:10–8.
  12. Zhang H, Wu Wenjia, Li Y, Liu Y, Wang J, Zhang B, Liu J. Polyelectrolyte microcapsules as ionic liquid reservoirs within ionomer membrane to confer high anhydrous proton conductivity. *J Power Sources.* 2015;279:667–77.
  13. Che Q, Sun B, He R. Preparation and characterization of new anhydrous, conducting membranes based on composites of ionic liquid trifluoroacetic propylamine and polymers of sulfonated poly (ether ether) ketone or polyvinylidene fluoride. *Electrochim Acta.* 2008;53:4428–34.
  14. Xu C, Liu X, Cheng J, Scott K. A polybenzimidazole/ionic-liquid-graphite-oxide composite membrane for high temperature polymer electrolyte membrane fuel cells. *J Power Sources.* 2015;274:922–7.
  15. Wang JT-W, Hsu SL-C. Enhanced high-temperature polymer electrolyte membrane for fuel cells based on polybenzimidazole and ionic liquids. *Electrochim Acta.* 2011;56:2842–6.
  16. Carrillo RH, Suarez-Guevara J, Torres-González LC, Gómez-Romero P, Sánchez EM. Incorporation of benzimidazolium ionic liquid in proton exchange membranes ABPBI–H<sub>3</sub>PO<sub>4</sub>. *J Mol Liq.* 2013;181:115–20.
  17. van de Ven E, Chairuna A, Merle G, Benito SP. Ionic liquid doped polybenzimidazole membranes for high temperature Proton Exchange Membrane fuel cell applications. *J Power Sources.* 2013;222:202–9.
  18. Blanco I, Cicala G, Latteri A, Mamo A, Recca A. Thermal and thermo-oxidative degradations of poly(2,6-dimethyl-1,4-phenylene oxide) (PPO)/copoly(aryl ether sulfone) P(ESES-co-EES) block copolymers: a kinetic study. *J Therm Anal Calorim.* 2013;112:375–81.
  19. Pasierb P, Gajerski R, Osiadly M, Łącz A. Application of DTA-TG-MS for determination of chemical stability of BaCeO<sub>3-δ</sub>-based protonic conductors. *J Therm Anal Calorim.* 2014;117:683–91.
  20. Ke HZ, Pang ZY, Peng B, Wang J, Cai YB, Huang FL, Wei QF. Thermal energy storage and retrieval properties of form-stable phase change nanofibrous mats based on ternary fatty acid eutectics/polyacrylonitrile composite by magnetron sputtering of silver. *J Therm Anal Calorim.* 2016;123:1293–307.
  21. Ortiz E, Pineres I, Leon C. On the low- to high proton-conducting transformation of a CsHSO<sub>4</sub>–CsH<sub>2</sub>PO<sub>4</sub> solid solution and its parents Physical or chemical nature? *J Therm Anal Calorim.* 2016;126:407–19.
  22. Dehabadi LL, Udoetok IA, Wilson LD. Macromolecular hydration phenomena: an overview of DSC studies on sulfonated tetrafluoroethylene-based fluoropolymer–copolymer (Nafion) and cellulose biopolymer materials. *J Therm Anal Calorim.* 2016;126:1851–66.
  23. Lis B, Dudek M, Kluczowski R, Krauz M, Kawalec M, Mosiałek M, Lach R. Physicochemical properties of ceramic tape involving Ca<sub>0.05</sub>Ba<sub>0.95</sub> Ce<sub>0.9</sub>Y<sub>0.1</sub>O<sub>3</sub> as an electrolyte designed for electrolyte-supported solid oxide fuel cells (IT-SOFCs). *J Therm Anal Calorim.* 2018. <https://doi.org/10.1007/s10973-018-7105-2>.
  24. Tofghi A, Rahimnejad M, Ghorbani M. Ternary nanotube a-MnO<sub>2</sub>/GO/AC as an excellent alternative composite modifier for cathode electrode of microbial fuel cell. *J Therm Anal Calorim.* 2018. <https://doi.org/10.1007/s10973-018-7198-7>.
  25. Toghyani S, Afshari E, Baniasadi E. Three-dimensional computational fluid dynamics modeling of proton exchange membrane electrolyzer with new flow field pattern. *J Therm Anal Calorim.* 2018. <https://doi.org/10.1007/s10973-018-7236-5>.
  26. Kitazawa Y, Iwata K, Kido R, Imaizumi S, Tsuzuki S, Shinoda W, Ueno K, Mandai T, Kokubo H, Dokko K, Watanabe M. Polymer electrolytes containing solvate ionic liquids: a new approach to achieve high ionic conductivity, thermal stability and a wide potential window. *Chem Mater.* 2018;30:252–61.
  27. Chen G, Chen N, Li L, Wang Q, Duan WF. Ionic liquid modified poly(vinyl alcohol) with improved thermal processability and excellent electrical conductivity. *Ind Eng Chem Res.* 2018;57:5472–81.
  28. Baczyńska M, Waszak M, Nowicki M, Prządka D, Borysiak S, Regel-Rosocka M. Characterization of polymer inclusion membranes (PIMs) containing phosphonium ionic liquids as Zn(II) carriers. *Ind Eng Chem Res.* 2018;57:5070–82.
  29. Li JS, Wang S, Xu JM, Xu LS, Liu FX, Tian X, Wang Z. Organic-inorganic composite membrane based on sulfonated poly (arylene ether ketone sulfone) with excellent long-term stability for proton exchange membrane fuel cells. *J Membr Sci.* 2017;529:243–51.
  30. Liu FX, Wang S, Li JS, Tian X, Wang X, Chen H, Wang Z. Polybenzimidazole/ionic-liquid-functional silica composite membranes with improved proton conductivity for high temperature proton exchange membrane fuel cells. *J Membr Sci.* 2017;541:492–9.
  31. Feng W, Lu Y, Chen Y, Lu Y, Yang T. Thermal stability of imidazolium-based ionic liquids investigated by TG and FTIR techniques. *J Therm Anal Calorim.* 2016;125(1):143–54.
  32. Lu Y, Cao Y, Lu Y, Yang T. Thermal stability and lifetime of [AMIM]Cl-PFSA composite membranes. *J Therm Anal Calorim.* 2017;128(3):1601–15.
  33. Kissinger HE. Variation of peak temperature with heating rate in differential thermal analysis. *J Res Natl Bur Stand.* 1956;57(4):217–21.
  34. Ozaw AT. A new method of analyzing thermogravimetric data. *Bull Chem Soc Jpn.* 1965;38(11):1881–6.
  35. Friedman HL. Kinetics of thermal degradation of char-forming plastics from thermogravimetry application to phenolic plastic. *J Polym Sci Part C Polym Symp.* 1964;6(1):183–95.
  36. Starink MJ. A new method for the derivation of activation energies from experiments performed at constant heating rate. *Thermochim Acta.* 1996;288(1/2):97–104.
  37. Hu R, Shi Q. Thermal analysis dynamics. 2nd ed. Beijing: Science Press; 2008. p. 151–5.
  38. Vyazovkin S, Burnham AK, Criado JM, Perez-Maqueda LA, Popescu C, Sbirrazzuoli N. ICTAC kinetics committee recommendations for performing kinetic computations on thermal analysis data. *Thermochim Acta.* 2011;520:1–19.
  39. Gotor FJ, Criado JM, Malek J, Koga N. Kinetic analysis of solid-state reactions: the Universality of master plots for analysing isothermal and non-isothermal experiments. *J Phys Chem A.* 2000;104:10777–8.